A multi-year timeseries of observation-based 3D horizontal and vertical quasi-geostrophic global ocean currents

Bruno Buongiorno Nardelli[1]

5 [1] Consiglio Nazionale delle Ricerche – Istituto di Scienze Marine, Napoli, 80133, Italy

Correspondence to: Bruno Buongiorno Nardelli (bruno.buongiornonardelli@cnr.it)

Abstract. Estimates of 3D ocean circulation are needed to improve our understanding of ocean dynamics and to assess its impact on marine ecosystems and Earth climate. Here we present the OMEGA3D product, an observation-based timeseries of (quasi) global 3D ocean currents covering the 1993-2018 period, developed by the Italian Consiglio Nazionale delle Ricerche
10 within the European Copernicus Marine Environment Monitoring Service (CMEMS). This dataset was obtained by applying a diabatic quasi-geostrophic (QG) diagnostic model to CMEMS data-driven ARMOR3D weekly reconstruction of temperature and salinity and ERA-Interim fluxes. Outside the equatorial band, vertical velocities were retrieved in the upper 1500 m, at nominal ¼° resolution, and successively used to compute the horizontal ageostrophic components. Root mean square differences between OMEGA3D total horizontal velocities and totally independent drifter observations at two different depths
15 (15 m and 1000 m) decrease with respect to corresponding estimates obtained from zero-order geostrophic balance, meaning that estimated vertical velocities can also be deemed reliable. OMEGA3D horizontal velocities are also closer to drifter observations than velocities provided by a set of re-analyses spanning a comparable time period, but based on data assimilation in ocean general circulation numerical models.

20 The full OMEGA3D product (released on 31st of March 2020) is available upon free registration at https://doi.org/10.25423/cmcc/multiobs_glo_phy_w_rep_015_007. The reduced subset used here for validation and review purposes is openly available at https://doi.org/10.5281/zenodo.3696885 (Buongiorno Nardelli, 2020).

1 Introduction

25 The recognition of the key role played by the oceans in the Earth system led the United Nations to proclaim the Decade of Ocean Science for Sustainable Development (2021-2030). Major efforts will consequently be put in the next years to analyse state-of-the-art observations and models and provide the indispensable knowledge basis to preserve the marine environment through effective science-informed policies. Providing accurate reconstructions of 3D ocean circulation timeseries is a fundamental part of this effort, aimed to better describe ocean dynamics and to assess its responses and feedbacks to natural
30 and anthropogenic pressures. However, assessing the time-evolving lateral and vertical transport of energy, momentum, gases,

nutrients, marine organisms and pollutants would require repeated synoptic observations of the 3D ocean state and surface forcings, that cannot be presently achieved even with the most advanced technologies. Hence, a combination of measurements collected from in situ and remote-sensing platforms and proper modelling frameworks are needed to describe the ocean circulation both in the ocean interior and at the domain boundaries. Two main complementary approaches can be followed to

35   this aim: the assimilation of observations in global ocean circulation numerical models (Carrassi et al., 2018; Moore et al., 2019; Stammer et al., 2016) and the combination of diagnostic models and purely data-driven reconstructions. The latter is presently more widely used for surface circulation retrievals, but its extension to 3D ocean state reconstruction is conveying a growing interest as advanced statistical and machine learning tools are becoming more computationally efficient (Buongiorno Nardelli et al., 2012; Buongiorno Nardelli and Santoleri, 2005; Guinehut et al., 2012; Lopez-Radcenco et al., 2018; Mulet et

40   al., 2012; Rio et al., 2016; Ubelmann et al., 2015; Yan et al., 2020). Both approaches present advantages and drawbacks: data assimilation in prognostic models may guarantee a description of the ocean state evolution that is fully consistent with the physics represented by the model, but the uncertainties in its initialization, the limits of the parameterizations of unresolved processes and the difficulties to properly represent model and observation errors and to account for their representativeness can significantly reduce models' ability to reproduce non-assimilated observations. Conversely, synergic use of satellite, in-

45   situ observations and data-driven reconstruction methodologies, in combination with simpler dynamical models (often limited to zero order balances, as in the retrieval of geostrophic currents from sea level data) can provide snapshots that better match independent observations (Mulet et al., 2012; Rio et al., 2016; Ubelmann et al., 2016).

The OMEGA3D product, developed by the *Consiglio Nazionale delle Ricerche* within the European Copernicus Marine Environment Monitoring Service (CMEMS) (product id=MULTIOBS_GLO_PHY_W_REP_015_007), delivers the first

50   observation-based retrievals of the global 3D vertical and horizontal ocean currents computed with a quasi-geostrophic (QG) model that explicitly considers the effect of both geostrophic advection and upper layer turbulent mixing. The data are provided weekly at 0.25° latitude-longitude resolution, with 75 non-uniformly spaced vertical levels between the surface and 1500 m depth, covering the period January 1993 to December 2018 (with planned yearly extensions based on updated upstream datasets). Outside the equatorial band, vertical velocities are obtained by solving a diabatic Q-vector formulation of the QG

55   Omega equation (Buongiorno Nardelli et al., 2018b; Giordani et al., 2006), with vertical mixing parameterized through the K-Profile Parameterization (KPP) (Smyth et al., 2002). Only once vertical velocities are known, the horizontal ageostrophic components can also be retrieved.

The accuracy of the QG velocities depends on the input data and on the theoretical limits of the model and parameterization used. Omega forcings are estimated here from the multi-year CMEMS product ARMOR3D (Guinehut et al., 2012), providing

60   a statistical reconstruction of 3D temperature and salinity fields from a combination of in situ profiles and satellite observations of sea surface temperature, salinity and topography. ERA-Interim air-sea fluxes are used to evaluate the forcing terms due to vertical mixing (Dee et al., 2011). QG approximation implies that Omega equation cannot be solved at the Equator, and increased errors are expected in the low latitude bands.

A direct validation of the vertical velocities is not possible due to the lack of direct reference observations. As such,

65   OMEGA3D vertical velocity mean pattern and variability have been compared here with the only global model re-analyses that presently include vertical velocity fields as disseminated output, namely Estimating the Circulation and Climate of the Ocean (ECCO) (Forget et al., 2015) and Simple Ocean Data Assimilation (SODA) (Carton et al., 2018).

Total horizontal and geostrophic components are instead compared with fully independent velocity estimates obtained from drifting buoys and Argo floats displacements. For reference, a similar comparison is carried out between two re-analyses,

70   SODA and CMEMS GLORYS (Drévillon et al., 2018) (GLobal Ocean ReanalYsis and Simulation), and drifter data.

2 Methods

2.1 Input datasets

Two datasets are taken in input to the OMEGA3D processing:

75   1) the   global ARMOR3D reprocessed dataset (Guinehut et al., 2012), distributed by CMEMS within product MULTIOBS_GLO_PHY_REP_015_002   (http://marine.copernicus.eu/services-portfolio/access-to-products/, dataset ID: dataset-armor-3d-rep-weekly), that is one of the two data-driven ocean state reconstructions included in the Ocean Reanalyses Intercomparison Project (ORA-IP) (Balmaseda et al., 2015). ARMOR3D is built in successive steps, that include the retrieval of temperature (T) and salinity (S) profiles from gap-free surface temperature (Reynolds et al., 2007), surface salinity (Droghei

80   et al., 2018) and sea level anomaly (AVISO+, 2015) fields, carried out through a multi-linear regression of historical profiles (Cabanes et al., 2013), and the successive combination of 3D synthetic fields with in-situ T/S profiles through an optimal interpolation algorithm. ARMOR3D provides weekly fields at nominal 0.25° latitude-longitude resolution, over 33 regularly spaced vertical levels, with different spacing depending on depth between the surface and 1500 m depth.

2) The ERA-Interim (Dee et al., 2011) surface air-sea fluxes, included in the global atmospheric reanalysis by the European

85   Centre   For   Medium-Range   Weather   Forecasts   (ECMWF,   https://apps.ecmwf.int/datasets/data/interim-full-daily/levtype=sfc/).

ERA-Interim assimilates several observations of upper-air atmospheric variables (e.g. satellite radiances, temperature, wind vectors, specific humidity, and ozone) through a four-dimensional variational (4D-VAR) system, running with a 12-hourly analysis cycle. OMEGA3D diabatic forcings take in input the mean daily fields of the zonal and meridional components of the

90   turbulent surface stress, the surface latent and heat flux, the surface net solar and thermal radiation, as well as total precipitation and evaporation (needed to estimate the equivalent surface salinity flux in KPP).

2.2 Input data pre-processing

The numerical tool used to retrieve OMEGA3D product is designed to run on a non-uniform vertical grid that displays a refined mesh close to the surface. The vertical layer thickness increases as the square of depth, and the final grid includes 75 vertical

95   levels between 2.5 m and 1482.5 m. This grid was specifically designed to get more accurate numerical solutions within the
      ocean upper boundary layer (Kalnay de Rivas, 1972; Sundqvist and Veronis, 1970). Pre-processing of input data thus includes
      as a first step the vertical interpolation of ARMOR3D data on OMEGA3D vertical layers (using *python* class
      scipy.interpolate.interp1d (Virtanen et al., 2019) set to cubic spline interpolation) and the mapping of ERA-Interim data on
      OMEGA3D horizontal grid (using *python* class *scipy.interpolate.griddata* (Virtanen et al., 2019), set to fit data to a piecewise
100   cubic, continuously differentiable, curvature-minimizing polynomial surface).

      As ARMOR3D data may occasionally display density inversions along the water column, that are not compatible with QG
      Omega solution, vertical profiles of potential density are adjusted to impose static stability: moving from the surface to depth,
      whenever a density inversion is found, density is set to the upper level value plus a 0.0001 kg/m^3 increment.

2.3 Quasi-Geostrophic equations

105   A diabatic Q-vector formulation of the quasi-geostrophic Omega equation (Buongiorno Nardelli et al., 2018b; Giordani et al.,
      2006) is solved to get the OMEGA3D vertical velocity fields:

$$\nabla^2{}_h (N^2 w) + f^2 \frac{\partial^2 w}{\partial z^2} = \nabla_h \cdot \boldsymbol{Q}$$

(1)

110   In Eq. (1), *w* represents the vertical velocity (positive upwards), N^2 is the Brunt–Väisälä frequency, *f* is the Coriolis parameter,
      h indicates the horizontal components, and the $\boldsymbol{Q}$ vector includes three components reflecting different processes (kinematic
      deformation, *twg*, turbulent buoyancy, *th*, and turbulent momentum, *dm*), as defined below:

$$\boldsymbol{Q} = 2\boldsymbol{Q}_{twg} + \boldsymbol{Q}_{th} + \boldsymbol{Q}_{dm}$$

115

$$\mathbf{Q}_{twg} = \frac{g}{\rho_0} \left(\frac{\partial u_g}{\partial x}\frac{\partial \rho}{\partial x} + \frac{\partial v_g}{\partial x}\frac{\partial \rho}{\partial y}, \frac{\partial u_g}{\partial y}\frac{\partial \rho}{\partial x} + \frac{\partial v_g}{\partial y}\frac{\partial \rho}{\partial y} \right)$$

$$\mathbf{Q}_{dm} = \frac{f}{\rho_0} \left(\frac{\partial^2}{\partial z^2}\rho \left[K_m \left(\frac{\partial v}{\partial z} - \gamma_v \right) \right], -\frac{\partial^2}{\partial z^2}\left[\rho K_m \left(\frac{\partial u}{\partial z} - \gamma_u \right) \right] \right)$$

$$\mathbf{Q}_{th} = -\frac{g}{\rho_0} \nabla_h \left(\frac{\partial}{\partial z}\left[K_\rho \left(\frac{\partial \rho}{\partial z} - \gamma_\rho \right) \right] \right) = \nabla_h \left(\frac{\partial}{\partial z}\left[K_\rho \left(N^2 + \frac{g}{\rho_0}\gamma_\rho \right) \right] \right)$$

(2)

      In the above definitions, ρ indicates the potential density, *g* is the gravitational acceleration, u_g and v_g represent the
120   geostrophic velocities, while turbulent terms are defined following the KPP parameterizations, namely through non-local
      effective gradients γ_x and classical viscosity/diffusivity K_x. The function used here to estimate KPP vertical mixing
      coefficients (Smyth et al., 2002) (only modified to handle derivatives in non-staggered non-uniform vertical grids) is designed

to account for Langmuir cells mixing by including an amplification of turbulent velocity scales, and includes a nonlocal momentum flux term and a parameterization of Stokes drift effects. Forcing terms are computed from ARMOR3D potential

125   density and geostrophic velocity fields, and ERA-interim atmospheric re-analyses.

In one of the analytical steps to obtain Eq. (1), the details on which are given elsewhere (Buongiorno Nardelli et al., 2018b; Giordani et al., 2006), the following two equations are found:

$$f^2 \frac{\partial u_a}{\partial z} = -\frac{\partial N^2 w}{\partial x} - 2f \left(\frac{\partial u_g}{\partial z} \frac{\partial v_g}{\partial x} + \frac{\partial v_g}{\partial z} \frac{\partial v_g}{\partial y} \right) + \frac{f}{\rho_0} \frac{\partial^2}{\partial z^2} \left(\rho K_m \left(\frac{\partial u}{\partial z} - \gamma_u \right) \right) - \frac{g}{\rho_0} \frac{\partial}{\partial x} \left(\frac{\partial}{\partial z} \left[K_\rho \left(N^2 + \frac{g}{\rho_0} \gamma_\rho \right) \right] \right)$$

130   (3a)

$$f^2 \frac{\partial v_a}{\partial z} = \frac{\partial N^2 w}{\partial y} + 2f \left(\frac{\partial u_g}{\partial z} \frac{\partial u_g}{\partial x} + \frac{\partial v_g}{\partial z} \frac{\partial u_g}{\partial y} \right) - \frac{f}{\rho_0} \frac{\partial^2}{\partial z^2} \left(\rho K_m \left(\frac{\partial v}{\partial z} - \gamma_u \right) \right) - \frac{g}{\rho_0} \frac{\partial}{\partial y} \left(\frac{\partial}{\partial z} \left[K_\rho \left(N^2 + \frac{g}{\rho_0} \gamma_\rho \right) \right] \right).$$

(3b)

Once vertical velocities are retrieved through Omega solution, these two equations allow to estimate also the horizontal

135   ageostrophic components (u_a and v_a) through a simple vertical integration of the right-hand side terms (assuming horizontal ageostrophic velocities are negligible at the bottom boundary).

2.4 Numerical solution

All equations used for the OMEGA3D retrieval are solved here numerically (Buongiorno Nardelli et al., 2018b). At each grid point in the interior domain (i.e. excluding the boundaries), the Omega equation is re-written substituting derivatives with

140   central finite differences, considering a non-staggered grid. Vertical derivatives are computed considering a variable grid spacing, increasing as the square of depth (Kalnay de Rivas, 1972), and adopting a second-order accuracy finite difference scheme (Sundqvist and Veronis, 1970).

At the surface and topographical boundaries Dirichelet conditions are imposed (namely zero vertical velocities) and Neumann conditions at the bottom and lateral boundaries (namely zero vertical velocity partial derivatives). These latter are imposed

145   through forward/backward finite schemes and make the solution not suited to model current topography interactions along the coasts. Grouping all factors multiplying w at each grid point one finally gets a set of equations that represent a closed linear system in w, which can thus be solved through a matrix inversion. Solving the linear system at once for the entire domain, however, would be computationally extremely demanding. As such, considering the elliptical nature of the Omega equation (which confines the impact of boundary conditions to a limited number of grid points), the original grid was split here in

150   smaller horizontally overlapping sub-domains (each tile having a horizontal dimension of 75 grid points, overlapping by one third). The inversion is carried out sequentially on these sub-domains, imposing the vertical velocity values that resulted from the previous step as lateral boundary conditions to the subsequent calculations. The algorithm used for the matrix inversion is

LGMRES (Baker et al., 2005) with incomplete LU preconditioning (as implemented in *python* sparse linear algebra package *scipy.sparse.linalg* (Virtanen et al., 2019)).

155   Vertical velocities are finally used to integrate Eq. (3) by a simple trapezoidal rule to obtain ageostrophic horizontal velocities.

3 Validation

3.1 Model re-analyses used for intercomparison

Three different ocean state reconstruction timeseries have been compared with OMEGA3D. All of them are based on ocean general circulation models assimilating both in situ and satellite observations, though significantly differing in term of

160   numerical schemes used, input data ingested and assimilation strategies.

The first dataset considered is the third release of version 4 of ECCO (Forget et al., 2015; Fukumori et al., 2018), hereafter ECCOv4r3, covering the 1992-2015 period, and available at https://ecco.jpl.nasa.gov/products/all/. ECCOv4r3 is based on the MIT General Circulation Model (Adcroft et al., 2001) and applies a 4D-VAR assimilation scheme to a wide set of observations (including satellite altimetry, in situ T/S profiles, satellite sea surface salinity and temperature, ocean bottom pressure)

165   (Fukumori et al., 2017), minimizing the observation-analysis misfits in a least squares sense (Wunsch and Heimbach, 2013). ECCOv4r3 model grid includes 50 vertical levels, with a zonal resolution of 1° and a variable meridional resolution, ranging from 1° to approximately 0.25° in the Equatorial band and near the poles. ECCOv4r3 is thus a relatively coarse resolution ocean circulation model and the effect of mesoscale dynamics on vertical velocities is parameterized by introducing a ''bolus'' vertical velocity (Danabasoglu et al., 1994; Gent and Mcwilliams, 1990; Liang et al., 2017), that needs to be added to the large-

170   scale Eulerian vertical velocity diagnosed from volume continuity. ECCOv4r3 vertical velocity data are released only as monthly averages (https://ecco.jpl.nasa.gov/products/V4r3/user-guide/).

The second dataset is version 3.4.2 of SODA (Carton et al., 2018), hereafter SODAv3.4.2, which covers the 1991-2017 period and can be downloaded from https://www.atmos.umd.edu/~ocean/. SODAv3.4.2 reanalysis is based on the ocean component of the NOAA/Geophysical Fluid Dynamics Laboratory CM2.5 coupled model (Delworth et al., 2012), namely version 5.1 of

175   Modular Ocean Model, and has been designed with a 0.25° horizontal and 50-level vertical resolution grid, thus improved with respect to previous versions of the same system (Carton et al., 2018) and providing the same nominal resolution of OMEGA3D. SODAv3.4.2 assimilates basic hydrographic data from World Ocean Database (Boyer et al., 2013) and level 3 (night-time) sea surface temperature from different sources (Carton et al., 2018) through a linear deterministic sequential filter, with a 10-day cycle. SODAv3.4.2 reanalysis output is provided on its native grid at 5-day resolution.

180   The third product used for the comparison is the output of the first version of the 1/12° horizontal resolution GLORYS system (Drévillon et al., 2018), hereafter GLORYS12v1, covering the period 1993-2018. GLORYS12v1 is obtained by jointly assimilating along track altimeter data, satellite SST, sea ice concentration and in situ temperature and salinity vertical profiles into a global ocean eddy-resolving model with 50 vertical levels. GLORYS12v1 model component is NEMO (Madec, 2016)

and data assimilation is carried out by means of a reduced-order Kalman filter, while a 3D-VAR scheme provides a correction
185   for the slowly-evolving large-scale biases in temperature and salinity.

GLORYS12v1   data   can   be   freely   downloaded   at: http://marine.copernicus.eu/services-portfolio/
(id=GLOBAL_REANALYSIS_PHY_001_030). GLORYS12v1 distributed output does not include vertical velocities. For the
sake of comparison, GLORYS12v1 daily files have been subsampled here over the same dates for which SODAv3.4.2 is
available.

190   As for OMEGA3D, ECCOv4r3, SODAv3.4.2 and GLORYS12v1 surface forcings are all taken from ERA-Interim (Dee et al.,
2011).

3.2 In situ validation data

Two fully independent in situ datasets have been considered for the validation of OMEGA3D horizontal velocities: Surface
Velocity Program (SVP) data (Lumpkin et al., 2013) from NOAA Global Drifter Program (covering the period 1993-2018 and
195   freely   available   at   https://www.aoml.noaa.gov/phod/gdp/)   and   YoMaHa'07   (Yoshinari Maximenko Hacker, hereafter
YOMAHA)   database   (Lebedev et al., 2007)   (covering   the   period   1997-2018   and   freely   available   at
http://apdrc.soest.hawaii.edu/projects/yomaha/). Both datasets provide velocity estimates obtained from the displacements of
drifting platforms along a Lagrangian trajectory.

In order to minimize wind slippage, SVP drifters are drogued with a 7 m long holey-sock centered at 15 m depth and their
200   velocity estimates is considered representative of currents at 15 m depth (Lumpkin et al., 2017). Before carrying out the
validation, individual SVP drifter 6-hourly records have been averaged over a running time window (inversely scaled with the
Coriolis parameter) to remove the signal due to inertial oscillations (Buongiorno Nardelli et al., 2018b).

YOMAHA velocities are estimated by measuring the displacement of profiling Argo floats during their submerged phase
(Lebedev et al., 2007). Argo floats drift at a pre-defined parking pressure and emerge only for near-real-time data transmission
205   through ARGOS/IRIDIUM satellites. Most of these instruments follow a profiling cycle of approximately 10 days, and their
parking level is set to 1000 m.

3.3 Vertical velocity mean patterns and resolved variability

Vertical velocities cannot be measured in the open ocean due to their relatively small magnitude (of the order of 1-100 m d^{-1},
depending on depth and processes involved). Consequently, OMEGA3D vertical velocity cannot be directly validated (no
210   reference datasets exist). However, the algorithm used to retrieve OMEGA3D horizontal velocities requires the vertical
velocity in input, and improvements in quasi-geostrophic horizontal components with respect to standard geostrophic velocities
would necessarily imply that vertical velocity is reliable.

OMEGA3D vertical velocities are thus compared here with the output of the only two ocean climate reanalysis systems that
presently distribute vertical velocity timeseries of comparable length. Considering that vertical velocity fields are provided at

215 different space-time resolutions, this comparison only describes the mean patterns and the amount of variability captured by each product.
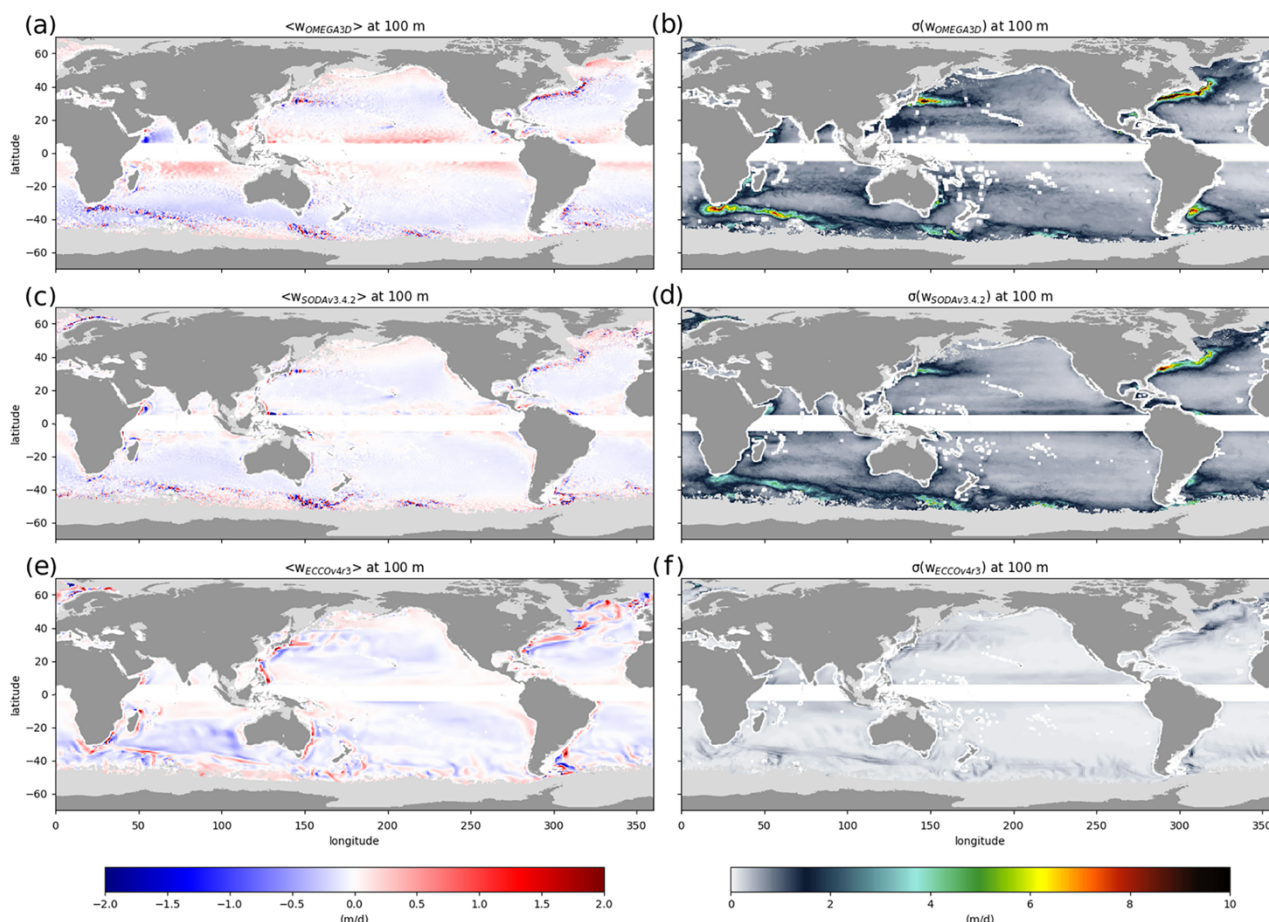
Figure 1. Mean vertical velocity at 100 m (a,c,e) and related standard deviation (b,d,f) computed from OMEGA3D (a,b), SODAv3.4.2 (c,d) and ECCOv4r3 (e,f) data on OMEGA3D domain over their 23 years overlapping period. Areas shallower than 100 m or 220 contaminated at least once by sea-ice within the averaging period are masked in light grey.
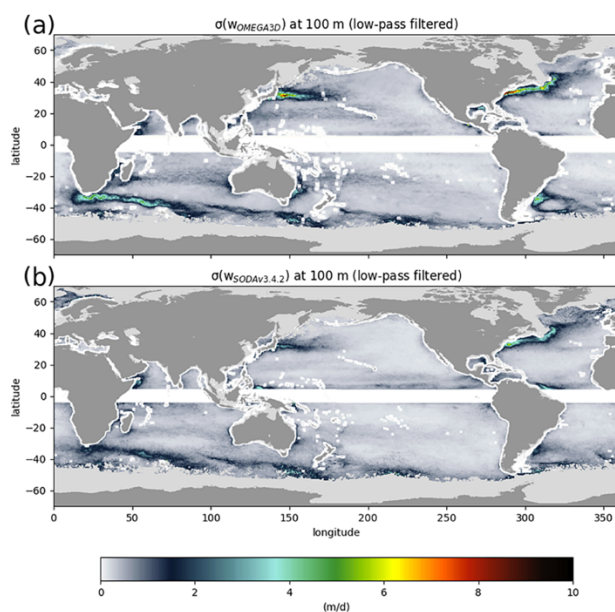
Specifically, mean vertical velocity patterns at 100 m depth and associated variability (standard deviation) are computed here from OMEGA3D, SODAv3.4.2 and ECCOv4r3 over their 23 years overlapping period (1993-2015), focusing on the domain covered by OMEGA3D product, thus excluding the 5°N-5°S band and coastal areas. The largescale patterns and range of 225 values found in the averaged velocities are quite similar among the three reconstructions (fig.1). Maximum absolute mean values reach around 2 m d^{-1} and areas dominated by large scale wind-driven upwelling at high latitudes and by downwelling at mid-latitudes are consistently identified in the three products, with values rarely exceeding 0.5 m d^{-1}. In the intertropical band, OMEGA3D vertical velocities display slightly higher values than the other two reconstructions (especially in the central

Open Access Earth System Science Data Discussions

Pacific). More substantial differences are found along the major Western boundary current systems and along the Antarctic
230   Circumpolar Current, where the different nominal resolution and the different dynamical representation of mesoscale features
in the three systems are reflected in terms of averaged vertical transport. Specifically, even if OMEGA3D and SODAv3.4.2
display very similar patterns, the former displays stronger values in the Agulhas return current and along the Gulf Stream
meanders, as well as around the northern branch of the anticyclonic gyre around the Zapiola Ridge, while the latter presents
intensified exchanges in the Pacific-Antarctic Ridge and South-Indian Ridge areas. As expected, ECCOv4r3 patterns do not
235   resolve any of the alternated upwelling/downwelling patterns found along the main currents' meanders in the two 0.25°
resolution products and its representation of mean vertical velocities in all western boundary currents basically consists in
uniform upwelling/downwelling associated with the parameterization of baroclinic instabilities along steep isopycnal slopes.
OMEGA3D mean vertical velocity patterns look very similar to SODAv3.4.2 also in the Northern part of the Atlantic Ocean,
while ECCOv4r3 presents quite different largescale patterns.

240

Figure 2. Mean monthly vertical velocity patterns and standard deviations computed from OMEGA3D (a), SODAv3.4.2 (b) after low-pass filtering the time series to remove signals above monthly frequency.

245   Given its 5-days sampling, SODAv3.4.2 could be expected to reveal a stronger variability than OMEGA3D (7-days sampling),
and both are expected to display much higher values than ECCOv4r3 (providing monthly averaged fields). Conversely, though
associated patterns display very similar features, OMEGA3D standard deviation maximum value exceeds SODAv3.4.2 by a
factor ~2. In both cases, intense maxima are associated with the main current systems.

For the sake of a more consistent comparison with ECCOv4r3, OMEGA3D and SODAv3.4.2 vertical velocity standard
250 deviations have also been estimated also after low-pass filtering both time series (by a 5-point and 7-point moving window,
respectively) to keep only frequencies lower than monthly (see figure 2). Even in that case, the variability observed in
ECCOv4r3 is sensibly lower than these retrieved from higher spatial resolution products, likely revealing the limits of the
mesoscale parameterization used in ECCOv4r3 in terms of vertical exchanges.

### 3.4 Horizontal velocity validation vs independent observations

255 OMEGA3D horizontal velocity accuracy has been assessed in terms of mean bias and root mean square differences (RMSD)
with respect to space-time co-located in situ reference observations. Estimated metrics have then been compared to that
estimated for geostrophic velocities directly obtained from DUACS altimeter data (AVISO+, 2015) (when looking at SVP
velocities) or from ARMOR3D (Mulet et al., 2012) (when looking at YOMAHA velocities), and successively also compared
to similar metrics computed from SODAv3.4.2 and GLORYS12v1 output.

260 To build our matchup databases, OMEGA3D velocities have been interpolated at the same nominal depth of drifter
measurements through a weighted average of the two closest levels.

The first assessment covered surface currents as measured by SVP drifters. As SVP may occasionally loose their drogue,
failing to correctly represent 15 m depth currents, only drogued SVP drifters data, collected within ±12 hours from nominal
reconstruction dates, have been included in our matchup databases (Fig.3a and 3b). The same matchup procedure has been

265 applied to DUACS geostrophic velocities, to SODAv3.4.2 and GLORYS12v1 (all of which share the same nominal horizontal
resolution).

Mean biases between SVP and OMEGA3D velocities (fig.4a) display similar values and patterns to what obtained from
altimeter-derived geostrophic velocities (fig.4c), with a slight underestimation of the current intensities. Overall, their mean
biases do not exceed 10 cm s^{-1}. GLORYS12v1 slightly overestimates mean western boundary currents, though displaying very

270 small biases elsewhere (fig.4e). Conversely, mean differences between SODAv3.4.2 at 15 m depth and SVP velocities (fig.4g)
reveal a more significant underestimation of surface currents, with biases reaching up to 20 cm s^{-1} over wide portions of the
domain. Similarly, OMEGA3D and DUACS RMSD (fig.6b and 6d) present very minor differences, while GLORYS12v1
presents significantly higher differences (by a factor ~1÷2) along all major currents (fig.4f). Even stronger discrepancies affect
SODAv3.4.2 estimates, displaying up to ~4 times higher RMSD values than OMEGA3D and DUACS along all major current

275 systems (fig.4h). It must be stressed that altimeter data are not assimilated in SODAv3.4.2, and modelled velocities are thus
less constrained by observations.

Directly comparing OMEGA3D and DUACS RMSD demonstrates that quasi-geostrophic velocities also improve with respect
to geostrophic velocities (by a few cm s^{-1}), mainly along the Antarctic Circumpolar Current and in the Western boundary
currents (fig.5a).
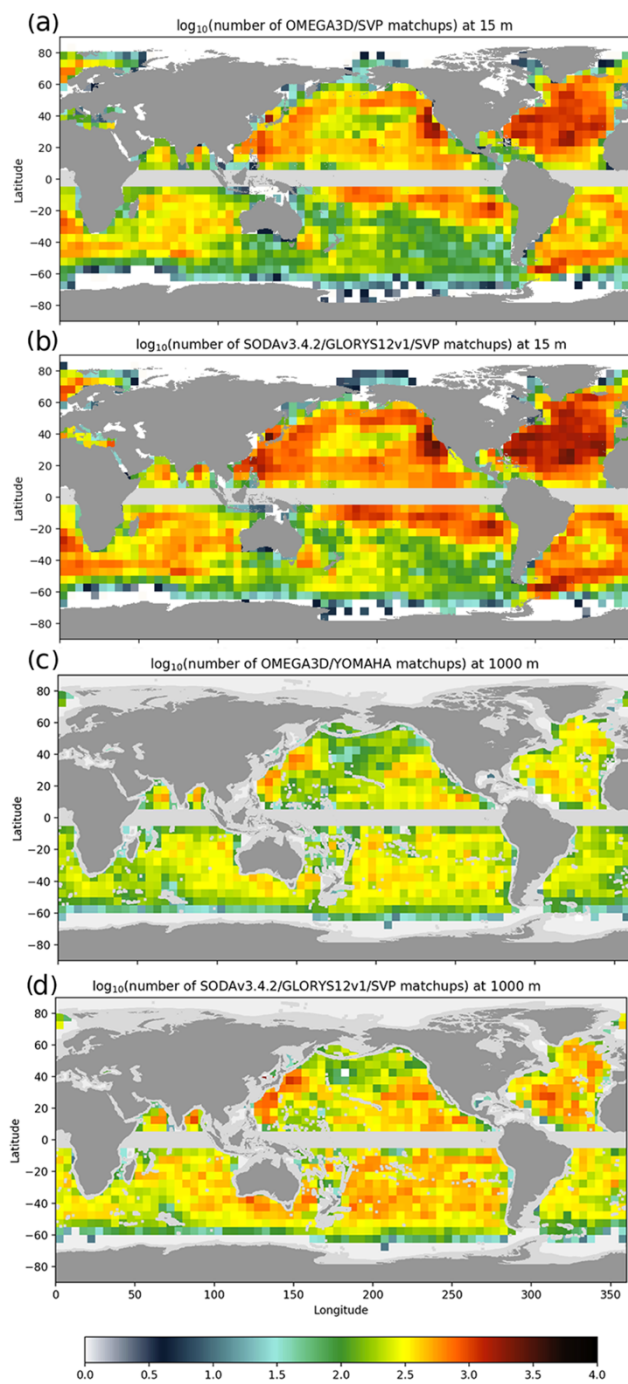
280

Figure 3. Number of matchups within 5°x5° bins between OMEGA3D (a) and GLORYS12v1/SODAv3.4.2 (b) velocities (at 15 m depth) and SVP observations, and between OMEGA3D (c) and GLORYS12v1/SODAv3.4.2 (d) velocities (at 1000 m) depth and YOMAHA velocities.
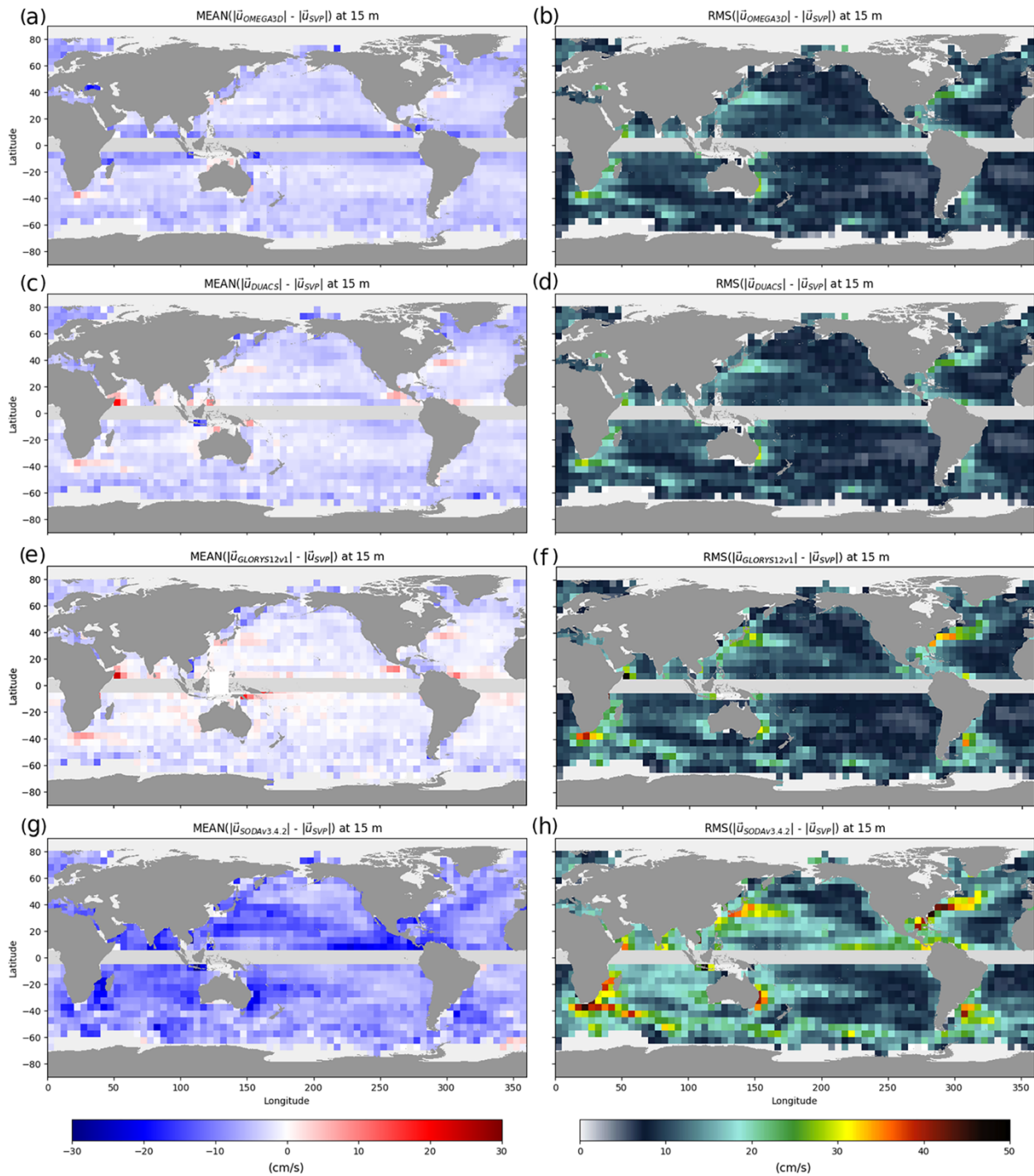
Figure 4: Mean and root mean square differences between OMEGA3D (a,b), DUACS (c,d), GLORYS12v1 (e,f), SODAv3.4.2 (g,h) velocities at 15 m depth and co-located SVP observations

285

Earth System
Science
Data

Open Access
Discussions
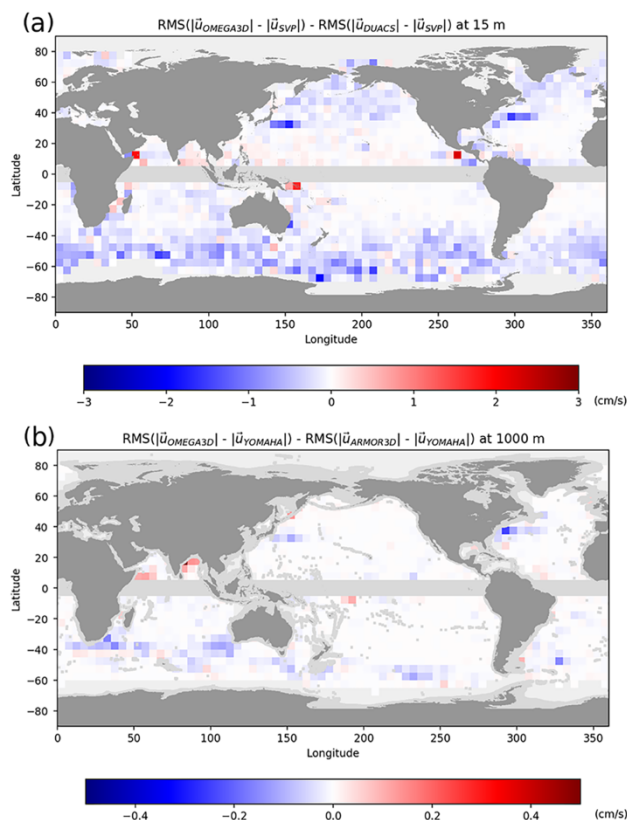
Figure 5. Difference between RMSD of OMEGA3D horizontal quasi-geostrophic and geostrophic velocities vs drifters in 5°x5° bins, at 15 m (a) and 1000 m (b) depth, respectively. Negative values indicate an improvement with respect to geostrophy.

The second assessment focused on velocities provided by YOMAHA dataset, which are representative of currents at 1000 m depth. In that case, in order to increase the number of samples, a temporal window of ±1 day has been considered to build the matchup database (Fig.3c and 3d).

Mean biases computed comparing any of the reconstructed currents with YOMAHA observations reveal a general overestimation of deep currents. The mean bias attains around 5 cm s^{-1} in OMEGA3D, ARMOR3D and GLORYS12v1 (fig.6a, 6c, 6e), while it gets up to >15 cm s^{-1} in SODAv3.4.2 (fig.6g). GLORYS12v1 displays more spatially homogeneous values (fig.6f), while purely observation-based values tend to overestimate mean western boundary currents but present slightly lower biases elsewhere (especially in the entire Atlantic Ocean). RMSD values computed from OMEGA3D, ARMOR3D and GLORYS12v1 at 1000 m depth (fig.6b, 6d, 6f) show extremely similar patterns and values. As for surface values, much stronger discrepancies are found between SODAv3.4.2 and YOMAHA estimates, reaching up to ~3 times higher RMSD values along the major current systems (fig.6h). Specific comparison of OMEGA3D and ARMOR3D, RMSD shows also in this case that quasi-geostrophic velocities improve with respect to geostrophic velocities, even if by only <0.5 cm s^{-1}, along the Antarctic Circumpolar Current and in the Western boundary currents (fig.5b).

305
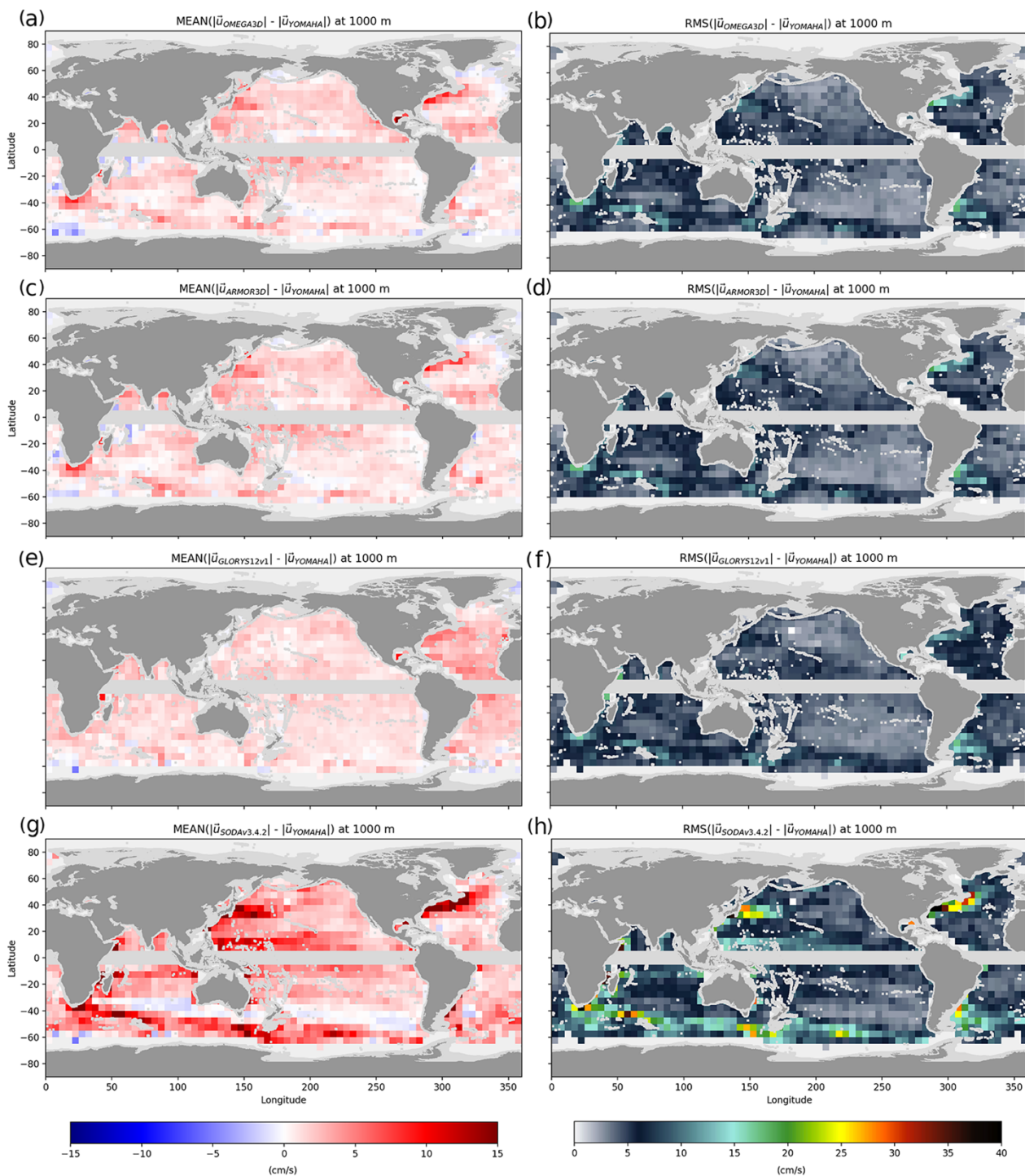
Figure 6: Mean and root mean square differences between OMEGA3D (a,b), ARMOR3D (c,d), GLORYS12v1 (e,f), SODAv3.4.2 (g,h) velocities at 1000 m depth and co-located YOMAHA observations.

4 Data availability

310 OMEGA3D product is distributed as part of the CMEMS catalogue (http://marine.copernicus.eu/services-portfolio/access-to-products/?option=com_csw&view=details&product_id=MULTIOBS_GLO_PHY_W_REP_015_007, https://doi.org/10.25423/cmcc/multiobs_glo_phy_w_rep_015_007). The reduced subset used for validation and review purposes is openly available at https://doi.org/10.5281/zenodo.3696885 (Buongiorno Nardelli, 2020). Access to the full product is granted after free registration as a user of CMEMS at http://marine.copernicus.eu/web/56-user-registration-

315 form.php. Once registered, users can download the product through a number of different tools/services, including: Web Portal Subsetter, Directgetfile (DGF), FTP. More information can be found at: http://marine.copernicus.eu/services-portfolio/technical-faq/.

The basic characteristics of OMEGA3D product are summarized in Table 1.

CMEMS Product ID	MULTIOBS_GLO_PHY_W_REP_015_007
Dataset ID	dataset-omega-3d-rep-weekly
Geographical coverage	89.875°S-89.875°N, 179.875°W-179.875°E equatorial band, coastal and ice-covered areas are masked
Temporal coverage	From 1993-01-06 to 2018-12-26 (weekly)
Spatial resolution	0.25° latitude-longitude regular grid 75 vertical layers (spacing increases as the square of depth) Depth range: 2.5-1482.5 m
Temporal resolution	Weekly fields (analysis centered on Wednesday at 00:00 UTC))
Variables	**uo** (m s^{-1}) quasi-geostrophic eastward velocity **vo** (m s^{-1}) quasi-geostrophic northward velocity **uago** (m s^{-1}) eastward ageostrophic velocity **vago** (m s^{-1}) northward ageostrophic velocity **wo** (m d^{-1}) quasi-geostrophic vertical velocity
Format/Conventions	Netcdf4/CF1.7

320 **Table 1. Main characteristics of CMEMS OMEGA3D product.**

15

Earth System
Science
Data

Open Access · Discussions

5 Conclusions

The 1993-2018 OMEGA3D timeseries provides weekly observation-based estimates of the 3D vertical and horizontal ocean currents in the upper 1500 m of the global oceans. The product is obtained by applying a quasi-geostrophic diagnostic model (based on the Omega equation) that includes the effect of both geostrophic advection and upper layer turbulent mixing and delivers, for the first time, estimates of the vertical velocities based on a combination of satellite and in situ observations. OMEGA3D timeseries is provided over a ¼° horizontal grid and inter-comparison with model re-analyses of comparable length and different space/time resolutions indicates that OMEGA3D resolves the highest amount of vertical velocity variance. OMEGA3D displays the smallest horizontal velocity root mean square differences with respect to independent estimates obtained from drifting buoys/floats displacements (when compared with re-analyses), mostly improving surface current estimates at the mid-high latitudes, along the Antarctic Circumpolar Current and in the Western boundary currents. Due to the approach followed to retrieve the horizontal ageostrophic components (once solved the Omega equation), the observed improvements (also with respect to simpler geostrophic estimates) mean that estimated vertical velocities should also be deemed reliable.

The model cannot be applied in the equatorial band (where QG approximation fails) and it does not include any parameterization of bottom boundary layer mixing. Dirichelet conditions are thus set at the bottom. As a consequence, considering also that the domain is limited in the vertical to the upper 1500 m, OMEGA3D is not suited for studies of bottom boundary dynamics and equatorial dynamics. Dirichelet conditions are applied also at coastal boundaries. Even if the effect of lateral boundary conditions only propagates a few grid points due to the elliptical nature of the Omega equation (Buongiorno Nardelli et al., 2001, 2012, 2018a), this makes OMEGA3D product not appropriate for studies of coastal dynamics either. As such, OMEGA3D is mostly suited to describe the role and long-term variability of open ocean large mesoscale dynamics and air-sea interactions (here parameterized through KPP), for example, on the vertical exchanges and water mass transformation outside the Equatorial band.

Author contribution.

The product described here has been designed and developed by BBN. All validation and inter-comparison exercises have been carried out by BBN. BBN has produced all figures and written the entire manuscript.

Competing interests.

The author declares that he has no conflict of interest.

Acknowledgements.

between Consiglio Nazionale delle Ricerche and Collecte Localisation Satellites (CLS), that is presently leading the CMEMS-

355 TAC-MOB. 83-CMEMS-TAC-MOB contract is funded by Mercator Ocean as part of its delegation agreement with the European Union, represented by the European Commission, to set-up and manage CMEMS.

References

Adcroft, A., Hill, C., Campin, J., Marshall, J., Heimbach, P., Initiative, M. I. T. C. M. and Ave, M.: Overview of the Formulation and Numerics of the MIT GCM, , 139–149, 2001.

360 AVISO+: SSALTO / DUACS User Handbook, CLS-DOS-NT-06-034, Issue 4.4, SALP-MU-P-EA-21065-CLS, 2015.

Baker, A. H., Jessup, E. R. and Manteuffel, T.: A technique for accelerating the convergence of restarted gmres, SIAM J. Matrix Anal. Appl., 26(4), 962–984, doi:10.1137/S0895479803422014, 2005.

Balmaseda, M. a., Hernandez, F., Storto, a., Palmer, M. D., Alves, O., Shi, L., Smith, G. C., Toyoda, T., Valdivieso, M., Barnier, B., Behringer, D., Boyer, T., Chang, Y.-S., Chepurin, G. a., Ferry, N., Forget, G., Fujii, Y., Good, S., Guinehut, S.,

365 Haines, K., Ishikawa, Y., Keeley, S., Köhl, a., Lee, T., Martin, M. J., Masina, S., Masuda, S., Meyssignac, B., Mogensen, K., Parent, L., Peterson, K. a., Tang, Y. M., Yin, Y., Vernieres, G., Wang, X., Waters, J., Wedd, R., Wang, O., Xue, Y., Chevallier, M., Lemieux, J.-F., Dupont, F., Kuragano, T., Kamachi, M., Awaji, T., Caltabiano, a., Wilmer-Becker, K. and Gaillard, F.: The Ocean Reanalyses Intercomparison Project (ORA-IP), J. Oper. Oceanogr., 8(sup1), s80–s97, doi:10.1080/1755876X.2015.1022329, 2015.

370 Boyer, T. P., Antonov, J. I., Baranova, O. K., Coleman, C., Garcia, H. E., Grodsky, A., Johnson, D. R., Locarnini, R. a, Mishonov, A. V, O'Brien, T. D., Paver, C. R., Reagan, J. R., Seidov, D., Smolyar, I. V, Zweng, M. M., Brien, T. D. O., Paver, C. R., Reagan, J. R., Seidov, D., Smolyar, I. V, Zweng, M. M. and Sullivan, K. D.: WORLD OCEAN DATABASE 2013, NOAA Atlas NESDIS 72, Sydney Levitus, Ed.; Alexey Mishonoc, Tech. Ed., NOAA Atlas, 209 pp, doi:10.7289/V5NZ85MT, 2013.

375 Buongiorno Nardelli, B. and Santoleri, R.: Methods for the Reconstruction of Vertical Profiles from Surface Data: Multivariate Analyses, Residual GEM, and Variable Temporal Signals in the North Pacific Ocean, J. Atmos. Ocean. Technol., 22(11), 1762–1781, doi:10.1175/JTECH1792.1, 2005.

Buongiorno Nardelli, B., Sparnocchia, S. and Santoleri, R.: Small mesoscale features at a meandering upper-ocean front in the Western Ionian Sea (Mediterranean Sea): Vertical motion and potential vorticity analysis, J. Phys. Oceanogr., (1995), 2227–

380 2250 [online] Available from: http://journals.ametsoc.org/doi/abs/10.1175/1520-0485(2001)031%3C2227:SMFAAM%3E2.0.CO%3B2 (Accessed 24 August 2013), 2001.

Buongiorno Nardelli, B., Guinehut, S., Pascual, a., Drillet, Y., Ruiz, S. and Mulet, S.: Towards high resolution mapping of 3-D mesoscale dynamics from observations, Ocean Sci., 8(5), 885–901, doi:10.5194/os-8-885-2012, 2012.

Buongiorno Nardelli, B., Mulet, S. and Iudicone, D.: Three-Dimensional Ageostrophic Motion and Water Mass Subduction

385 in the Southern Ocean, J. Geophys. Res. Ocean., 1–30, doi:10.1002/2017JC013316, 2018a.

Buongiorno Nardelli, B., Mulet, S. and Iudicone, D.: Three dimensional ageostrophic motion and water mass subduction in the Southern Ocean, J. Geophys. Res. Ocean., 2018b.

Buongiorno Nardelli, B.: CNR global observation-based OMEGA3D quasi-geostrophic vertical and horizontal ocean currents (1993-2018): validation subset. (Version V1.0) [Data set]. Zenodo. http://doi.org/10.5281/zenodo.3696885, 2020.

390   Cabanes, C., Grouazel, a., von Schuckmann, K., Hamon, M., Turpin, V., Coatanoan, C., Paris, F., Guinehut, S., Boone, C., Ferry, N., de Boyer Montégut, C., Carval, T., Reverdin, G., Pouliquen, S. and Le Traon, P.-Y.: The CORA dataset: validation and diagnostics of in-situ ocean temperature and salinity measurements, Ocean Sci., 9(1), 1–18, doi:10.5194/os-9-1-2013, 2013.

Carrassi, A., Bocquet, M., Bertino, L. and Evensen, G.: Data assimilation in the geosciences: An overview of methods, issues,
395   and perspectives, Wiley Interdiscip. Rev. Clim. Chang., 9(5), 1–50, doi:10.1002/wcc.535, 2018.

Carton, J. A., Chepurin, G. A. and Chen, L.: SODA3: A New Ocean Climate Reanalysis, J. Clim., 31(17), 6967–6983, doi:10.1175/jcli-d-18-0149.1, 2018.

Danabasoglu, G., McWilliams, J. C. and Gent, P. R.: The role of mesoscale tracer transports in the global ocean circulation, Science (80-.)., 264(5162), 1123–1126, doi:10.1126/science.264.5162.1123, 1994.

400   Dee, D. P., Uppala, S. M., Simmons, A. J., Berrisford, P., Poli, P., Kobayashi, S., Andrae, U., Balmaseda, M. A., Balsamo, G., Bauer, P., Bechtold, P., Beljaars, A. C. M., Berg, L. Van De, Bidlot, J., Bormann, N., Delsol, C., Dragani, R., Fuentes, M., Geer, A. J. and Dee, D. P.: The ERA-Interim reanalysis : configuration and performance of the data assimilation system, , (April), 553–597, doi:10.1002/qj.828, 2011.

Delworth, T. L., Rosati, A., Anderson, W., Adcroft, A. J., Balaji, V., Benson, R., Dixon, K., Griffies, S. M., Lee, H. C.,
405   Pacanowski, R. C., Vecchi, G. A., Wittenberg, A. T., Zeng, F. and Zhang, R.: Simulated climate and climate change in the GFDL CM2.5 high-resolution coupled climate model, J. Clim., 25(8), 2755–2781, doi:10.1175/JCLI-D-11-00316.1, 2012.

Drévillon, M., Régnier, C., Lellouche, J.-M., Garric, G., Bricaud, C. and Hernandez, O.: CMEMS Quality Information Document for Global Ocean Reanalysis Products -GLOBAL-REANALYSIS-PHY-001-030, CMEMS-GLO-QUID-001-030., 2018.

410   Droghei, R., Buongiorno Nardelli, B. and Santoleri, R.: A New Global Sea Surface Salinity and Density Dataset From Multivariate Observations (1993–2016), Front. Mar. Sci., 5(March), 1–13, doi:10.3389/fmars.2018.00084, 2018.

Forget, G., Campin, J. M., Heimbach, P., Hill, C. N., Ponte, R. M. and Wunsch, C.: ECCO version 4: An integrated framework for non-linear inverse modeling and global ocean state estimation, Geosci. Model Dev., 8(10), 3071–3104, doi:10.5194/gmd-8-3071-2015, 2015.

415   Fukumori, I., Wang, O., Fenty, I., Forget, G., Heimbach, P. and Ponte, R. M.: ECCO Version 4 Release 3, Dspace.Mit.Edu, 2(2015), 10, doi:1721.1/110380, 2017.

Fukumori, I., Heimbach, P., Ponte, R. M. and Wunsch, C.: A dynamically consistent, multivariable ocean climatology, Bull. Am. Meteorol. Soc., 99(10), 2107–2127, doi:10.1175/BAMS-D-17-0213.1, 2018.

Gent, P. R. and Mcwilliams, J. C.: Isopycnal Mixing in Ocean Circulation Models, J. Phys. Oceanogr., 20(1), 150–155,

Earth System
Science Data
Open Access Discussions

420 doi:10.1175/1520-0485(1990)020<0150:IMIOCM>2.0.CO;2, 1990.

Giordani, H., Prieur, L. and Caniaux, G.: Advanced insights into sources of vertical velocity in the ocean, Ocean Dyn., 56(5–6), 513–524, doi:10.1007/s10236-005-0050-1, 2006.

Guinehut, S., Dhomps, a.-L., Larnicol, G. and Le Traon, P.-Y.: High resolution 3-D temperature and salinity fields derived from in situ and satellite observations, Ocean Sci., 8(5), 845–857, doi:10.5194/os-8-845-2012, 2012.

425 Kalnay de Rivas, E.: On the use of nonuniform grids in finite-difference equations, J. Comput. Phys., 10, 202–210, 1972.

Lebedev, K. V, Yoshinari, H., Maximenko, N. A. and Hacker, P. W.: Velocity data assessed from trajectories of Argo floats at parking level and at the sea surface, IPRC Tech. Note, 4(2), 20, 2007.

Liang, X., Spall, M. and Wunsch, C.: Global Ocean Vertical Velocity From a Dynamically Consistent Ocean State Estimate, J. Geophys. Res. Ocean., 1–17, doi:10.1002/2017JC012985, 2017.

430 Lopez-Radcenco, M., Pascual, A., Gomez-Navarro, L., Aissa-El-Bey, A. and Fablet, R.: Analog data assimilation for along-track nadiR and SWOT altimetry data in the western Mediterranean Sea, Int. Geosci. Remote Sens. Symp., 2018-July, 7684–7687, doi:10.1109/IGARSS.2018.8519089, 2018.

Lumpkin, R., Grodsky, S. A., Centurioni, L., Rio, M. H., Carton, J. A. and Lee, D.: Removing spurious low-frequency variability in drifter velocities, J. Atmos. Ocean. Technol., 30(2), 353–360, doi:10.1175/JTECH-D-12-00139.1, 2013.

435 Lumpkin, R., Özgökmen, T. and Centurioni, L.: Advances in the Application of Surface Drifters, Ann. Rev. Mar. Sci., 9(1), 59–81, doi:10.1146/annurev-marine-010816-060641, 2017.

Madec, G.: NEMO ocean engine., 2016.

Moore, A. M., Martin, M. J., Akella, S., Arango, H. G., Balmaseda, M., Bertino, L., Ciavatta, S., Cornuelle, B., Cummings, J., Frolov, S., Lermusiaux, P., Oddo, P., Oke, P. R., Storto, A., Teruzzi, A., Vidard, A. and Weaver, A. T.: Synthesis of Ocean

440 Observations Using Data Assimilation for Operational, Real-Time and Reanalysis Systems: A More Complete Picture of the State of the Ocean, Front. Mar. Sci., 6(March), 1–6, doi:10.3389/fmars.2019.00090, 2019.

Mulet, S., Rio, M.-H., Mignot, a., Guinehut, S. and Morrow, R.: A new estimate of the global 3D geostrophic ocean circulation based on satellite data and in-situ measurements, Deep Sea Res. Part II Top. Stud. Oceanogr., 77–80, 70–81, doi:10.1016/j.dsr2.2012.04.012, 2012.

445 Reynolds, R. W., Smith, T. M., Liu, C., Chelton, D. B., Casey, K. S. and Schlax, M. G.: Daily High-Resolution-Blended Analyses for Sea Surface Temperature, J. Clim., 20(22), 5473–5496, doi:10.1175/2007JCLI1824.1, 2007.

Rio, M.-H., Santoleri, R. and Bourdalle-Badie, R.: Improving the Altimeter-Derived Surface Currents Using High-Resolution Sea Surface Temperature Data : A Feasability Study Based on Model Outputs, , 2769–2784, doi:10.1175/JTECH-D-16-0017.1, 2016.

450 Smyth, W. D., Skyllingstad, E. D., Crawford, G. B. and Wijesekera, H.: Nonlocal fluxes and Stokes drift effects in the K-profile parameterization, Ocean Dyn., 52(3), 104–115, doi:10.1007/s10236-002-0012-9, 2002.

Stammer, D., Balmaseda, M., Heimbach, P., Köhl, A. and Weaver, A.: Ocean Data Assimilation in Support of Climate Applications: Status and Perspectives, Ann. Rev. Mar. Sci., 8(1), annurev-marine-122414-034113, doi:10.1146/annurev-

Earth System
Science
Data

Open Access

Discussions

marine-122414-034113, 2016.

455 Sundqvist, H. and Veronis, G.: A simple finite-difference grid with non-constant intervals, Tellus, XXII, 1–6 [online] Available from: http://onlinelibrary.wiley.com/doi/10.1111/j.2153-3490.1970.tb01933.x/abstract (Accessed 26 August 2013), 1970.

Ubelmann, C., Klein, P. and Fu, L.-L.: Dynamic Interpolation of Sea Surface Height and Potential Applications for Future High-Resolution Altimetry Mapping, J. Atmos. Ocean. Technol., 32(1), 177–184, doi:10.1175/JTECH-D-14-00152.1, 2015.

Ubelmann, C., Cornuelle, B. D. and Fu, L.-L.: Dynamic Mapping of Along-Track Ocean Altimetry : Method and Performance

460 from Observing System Simulation Experiments, , 33, 1691–1699, doi:10.1175/JTECH-D-15-0163.1, 2016.

Virtanen, P., Gommers, R., Oliphant, T. E., Haberland, M., Reddy, T., Cournapeau, D., Burovski, E., Peterson, P., Weckesser, W., Bright, J., van der Walt, S. J., Brett, M., Wilson, J., Millman, K. J., Mayorov, N., Nelson, A. R. J., Jones, E., Kern, R., Larson, E., Carey, C., Polat, İ., Feng, Y., Moore, E. W., VanderPlas, J., Laxalde, D., Perktold, J., Cimrman, R., Henriksen, I., Quintero, E. A., Harris, C. R., Archibald, A. M., Ribeiro, A. H., Pedregosa, F., van Mulbregt, P. and Contributors, S. 1. 0:

465 SciPy 1.0--Fundamental Algorithms for Scientific Computing in Python, , 1–22 [online] Available from: http://arxiv.org/abs/1907.10121, 2019.

Wunsch, C. and Heimbach, P.: Dynamically and kinematically consistent global ocean circulation and ice state estimates, 2nd ed., Elsevier Ltd., 2013.

Yan, Z., Wu, B., Li, T., Collins, M., Clark, R., Zhou, T., Murphy, J. and Tan, G.: Eastward shift and extension of ENSO-

470 induced tropical precipitation anomalies under global warming, , (January), 1–11, 2020.